



HAL
open science

Uncertainty analysis and validation of the estimation of effective hydraulic properties at the Darcy scale

Arnaud Mesgouez, Samuel Buis, Stéphane Ruy, Gaëlle Lefeuvre-Mesgouez

► **To cite this version:**

Arnaud Mesgouez, Samuel Buis, Stéphane Ruy, Gaëlle Lefeuvre-Mesgouez. Uncertainty analysis and validation of the estimation of effective hydraulic properties at the Darcy scale. *Journal of Hydrology*, 2014, 512, pp.303-314. 10.1016/j.jhydrol.2014.02.065 . hal-00793526v4

HAL Id: hal-00793526

<https://hal.science/hal-00793526v4>

Submitted on 24 Mar 2014

HAL is a multi-disciplinary open access archive for the deposit and dissemination of scientific research documents, whether they are published or not. The documents may come from teaching and research institutions in France or abroad, or from public or private research centers.

L'archive ouverte pluridisciplinaire **HAL**, est destinée au dépôt et à la diffusion de documents scientifiques de niveau recherche, publiés ou non, émanant des établissements d'enseignement et de recherche français ou étrangers, des laboratoires publics ou privés.

Uncertainty analysis and validation of the estimation of effective hydraulic properties at the Darcy scale

A. Mesgouez^{a,b,*}, S. Buis^{b,a}, S. Ruy^{b,a}, G. Lefeuvre-Mesgouez^{a,b}

^a*Université d'Avignon et des Pays de Vaucluse, UMR1114 EMMAH, Faculté des Sciences, F-84000 Avignon, France*

^b*INRA, UMR1114 EMMAH, F-84914 Avignon, France*

Abstract

The determination of the hydraulic properties of heterogeneous soils or porous media remains challenging. In the present study, we focus on determining the effective properties of heterogeneous porous media at the Darcy scale with an analysis of their uncertainties.

Preliminary, experimental measurements of the hydraulic properties of each component of the heterogeneous medium are obtained. The properties of the effective medium, representing an equivalent homogeneous material, are determined numerically by simulating a water flow in a three-dimensional representation of the heterogeneous medium, under steady-state scenarios and using its component properties. One of the major aspects of this study is to take into account the uncertainties of these properties in the computation and evaluation of the effective properties. This is done using a bootstrap method.

*Corresponding author

Email addresses: arnaud.mesgouez@univ-avignon.fr (A. Mesgouez),
sbuis@avignon.inra.fr (S. Buis), ruy@avignon.inra.fr (S. Ruy),
gaelle.mesgouez@univ-avignon.fr (G. Lefeuvre-Mesgouez)

Numerical evaporation experiments are conducted both on the heterogeneous and on the effective homogeneous materials to evaluate the effectiveness of the proposed approach. First, the impact of the uncertainties of the component properties on the simulated water matric potential is found to be high for the heterogeneous material configuration. Second, it is shown that the strategy developed herein leads to a reduction of this impact. Finally, the adequacy between the mean of the simulations for the two configurations confirms the suitability of the homogenization approach, even in the case of dynamic scenarios.

Although it is applied to green roof substrates, a two-component media composed of bark compost and pozzolan used in the construction of buildings, the methodology proposed in this study is generic.

Keywords: effective hydraulic parameters, heterogeneous porous media, uncertainty estimation, green roof substrate, the Richards equation, bootstrapping method

1. Introduction

At the Darcy scale, heterogeneous media can be represented in different ways. Basically, a heterogeneous medium can be modeled either using a spatial distribution of properties inside a single unit (Khaleel et al., 2002; Mantoglou and Gelhar, 1987; Russo, 1992; Vogel et al., 2010; Yeh et al., 1985 among others), or using a patchwork of homogeneous sub-units (Bechtold et al., 2012; Samouëlian et al., 2011; Wildenschild and Jensen, 1999a). A combination of both approaches (Javaux and Vanclooster, 2006a; Zhang et al., 2010) can also be used. A detailed description of the various representations

10 can be found in the reviews of Renard and de Marsily (1997) or Vereecken et
11 al. (2007). In our study, we refer to the second way of representation, based
12 on a patchwork of homogeneous sub-units.

13 The determination of these sub-units is a difficult task and can be per-
14 formed in different ways. Invasive methods for delineating three-dimensional
15 natural soil units include pedological or geological observations (Bierkens
16 and van der Gaast, 1998; Javaux and Vanclooster, 2006b ; Ma et al., 2010
17 ; Samouëlian et al., 2011) and dye tracing experiments (Javaux and Van-
18 clooster, 2006a). Non invasive methods such as two-dimensional electrical
19 resistivity tomography (Besson et al., 2004; Tabbagh et al., 2000) or three-
20 dimensional x-ray computed assist tomography (Duliu, 1999) can also be
21 used. The alternative approach is to work on remolded porous media, such
22 as calibrated sands, to precisely control the heterogeneity pattern and the
23 distribution of hydraulic properties (Bechtold et al., 2012; Danquigny and
24 Ackerer, 2005; Wildenschild and Jensen, 1999b). In our study, we refer to
25 this last way of representation.

26 When working on a patch of homogeneous sub-units, each component
27 of the heterogeneous medium is considered as a single-phase continuum de-
28 scribed by macroscopic laws (the Darcy law and the Richards equation). Wa-
29 ter flow simulation or water balance computation can then be performed on
30 the elementary volume by using a numerical solver of the Richards equation
31 accounting for the spatial heterogeneity of the hydraulic properties. The
32 spatial structure must be known to distribute the hydraulic properties of
33 each material on the volume of interest. Moreover, solving the Richards
34 equation can be tedious, in particular for three-dimensional flow in complex

35 heterogeneous geometry (Herbst et al., 2008). A simpler approach consists
36 in replacing the explicit three-dimensional structure of the heterogeneous
37 volume by a homogeneous medium, wherein the properties of the homoge-
38 nized medium take into account the hydraulic properties of each material, in
39 such a way that simulations conducted on both domains yield similar water
40 fluxes under identical boundary conditions (Samouëlian et al., 2011). Such
41 medium properties are then called effective properties. The effective medium
42 is still obtained at the Darcy scale. The homogenization approach can then
43 be considered as an upscaling technique from a continuum scale to a larger
44 continuum one.

45 Due to the recent advances in computing capabilities, numerical ap-
46 proaches are now widely used for the determination of effective properties
47 (Samouëlian et al., 2007; Vogel et al., 2010). The objective of this study
48 is to contribute to the evaluation of this approach. Several authors noted
49 that simulations conducted using effective parameters may differ from simu-
50 lations conducted with spatially distributed parameters (Vogel et al., 2008;
51 Vogel et al., 2010) or from experimental data measured on heterogeneous me-
52 dia (Wildenschild and Jensen, 1999b). In addition, though several authors
53 estimated the effective hydraulic properties of various natural soils (Javaux
54 and Vanclooster, 2006a; Samouëlian et al., 2011; Vogel and Roth, 1998), no
55 study, to our knowledge, integrates a complete uncertainty evaluation of this
56 procedure. The process of estimating the hydraulic properties of a given
57 material includes however various sources of uncertainties (Mohrath et al.,
58 1997; Peters and Durner, 2008; see also section 2.2 of this article). These
59 uncertainties significantly affect the results of numerical simulations (Chris-

60 tiaens and Feyen, 2001; Coppola et al., 2009; Pan et al., 2009) and thus the
61 estimation of effective properties or their evaluation using dynamic scenar-
62 ios. In this study, we propose to estimate the uncertainties on the effective
63 hydraulic properties of a real heterogeneous material, and to evaluate these
64 properties and the impact of their uncertainties by comparing simulations
65 of a dynamic process using either the heterogeneous medium or the effective
66 homogeneous material.

67 The methodology proposed in this article is generic. It is applied here to
68 green roof substrates, hereafter called substrate or complex substrate. It is a
69 composite of compressible materials, namely organic matter (bark compost)
70 used as fertilizer, and of aggregates of volcanic rock (pozzolan) used as rigid
71 skeleton. This two-component material is considered to serve a number of
72 beneficial purposes that can help in the management of various environmen-
73 tal problems, such as the reduction of air pollution or of the carbon footprints
74 of cities (Yang et al., 2008), the improvement of storm water management
75 (Carter and Jackson, 2007) and the improvement of energy efficiency in build-
76 ings (Ouldboukhitine et al., 2012).

77 **2. Materials and Methods**

78 The methodology followed in this study is sketched up in Fig. 1. The
79 heterogeneous material under study is composed of a combination of bark
80 compost and pozzolan. In the first step, water retention and hydraulic con-
81 ductivity are measured for both materials using ad hoc experimental pro-
82 cedures for different water matric potential and on different samples. The
83 hydraulic properties are then estimated by fitting parametric models to the

84 experimental data. The uncertainties on these properties are estimated using
85 a bootstrap method.

86 In the second step, effective hydraulic parameters are determined by simu-
87 lating numerically the water flow in a three-dimensional representation of the
88 heterogeneous material taking into account the uncertainties on the hydraulic
89 properties of each constitutive materials and on the spatial distribution of
90 the materials using Monte Carlo random sampling. The effective hydraulic
91 properties and associated uncertainties are then estimated in the same way
92 as for single material properties but using the simulated water retention and
93 conductivity values.

94 Finally, in the third step, the reliability of the computed effective hy-
95 draulic properties is evaluated. Simulations of the evolution of water matric
96 potential versus time are performed under dynamic scenarios with the ef-
97 fective medium and the heterogeneous material taking into account the un-
98 certainties on their hydraulic properties and the spatial distribution of the
99 materials. Their mean behaviors are cross-checked and the impact of the
100 uncertainties is compared.

101 The following subsections give details on the models used for fitting hy-
102 draulic properties, the methodology followed for estimating their uncertain-
103 ties, the numerical configuration of the water flow simulations, the method
104 used for computing the effective properties and the evaluation of the homog-
105 enization approach. The experimental procedures used for measuring water
106 retention and hydraulic conductivity for bark compost and pozzolan and the
107 specific C++ parallelized code used for solving the Richards equation are
108 described in Appendix A and B respectively.

109 *2.1. Models of hydraulic properties*

110 The van Genuchten model (van Genuchten, 1980) is fitted to the exper-
 111 imental data to obtain the hydraulic properties, from which we deduce the
 112 water retention curve, i.e. the relation between $\theta(h, \mathbf{x}, t)$ [$L^3 L^{-3}$], the volu-
 113 metric water content, and $h(\mathbf{x}, t)$ [L], the water matric potential, as follows

$$\theta(h, \mathbf{x}, t) = \theta_r(\mathbf{x}) + (\theta_s(\mathbf{x}) - \theta_r(\mathbf{x})) \times \left[1 + \left(\frac{h(\mathbf{x}, t)}{h_e(\mathbf{x})} \right)^n \right]^{-m} \quad (1)$$

114 where \mathbf{x} [L] are the spatial coordinates, t [T] is the time, θ_r [$L^3 L^{-3}$] is the
 115 residual volumetric water content, θ_s [$L^3 L^{-3}$] is the water content at satura-
 116 tion, h_e [L] is a scale parameter, n [-] and m [-] are shape parameters with
 117 $m = 1 - 1/n$.

118 The Mualem-van Genuchten model (van Genuchten, 1980) is fitted to the
 119 experimental data to obtain the hydraulic properties, from which we deduce
 120 the hydraulic conductivity curve, i.e. the relation between $K(h, \mathbf{x}, t)$ [LT^{-1}],
 121 the hydraulic conductivity, and $h(\mathbf{x}, t)$, the matric water potential, as follows

$$K(h, \mathbf{x}, t) = K_{Sat}(\mathbf{x}) \cdot \frac{[1 - (h(\mathbf{x}, t)/h_e(\mathbf{x}))^{n-1} \times (1 + (h(\mathbf{x}, t)/h_e(\mathbf{x}))^n)^{-m}]^2}{[1 + (h(\mathbf{x}, t)/h_e(\mathbf{x}))^n]^{m/2}} \quad (2)$$

122 The values of the parameters of the hydraulic models are estimated by fit-
 123 ting these models on all the available observations. These fits are performed
 124 using non-linear least squares regression with a trust-region-reflective mini-
 125 mizer (Coleman and Li, 1996). The method of estimating the uncertainties
 126 for these properties is detailed in the following subsection.

127 *2.2. Uncertainty evaluation methodology*

128 As already mentioned, various approximations and errors can be sources
129 of uncertainty when estimating the hydraulic properties of a material. The
130 following typology is proposed to classify these sources of uncertainty:

- 131 1. Variability in the properties of samples: owing to the variability of the
132 material samples used in some experiments, or due to the fact that some
133 experiments result in the destruction of the samples, measurements of
134 the properties of a material are often performed on replicates. The
135 number of replicates may have a significant impact on the estimation
136 of the hydraulic properties of a material depending on the level of their
137 individual variability.
- 138 2. Errors in experimental data due to (i) approximations used for size
139 characterization, weight or density measurements, sensor locations, and
140 to (ii) digitalization errors associated with digital data-loggers. These
141 errors can propagate in the estimation of the hydraulic properties as
142 noted by Tamari et al. (1993).
- 143 3. Model errors due to inadequate model assumptions. Vogel et al. (2010)
144 showed in a numerical case study that the validation of the homoge-
145 nization process requires a highly flexible hydraulic law model.
- 146 4. Fitting errors: in the presence of a low number of experimental data,
147 the level of uncertainty of the obtained parameters using parametric
148 models fitted to the experimental data may be very high, even in case
149 of slight variability in the properties of the samples and of slight mea-
150 surement errors.

151 In our study the bootstrap method (Efron and Tibshirani, 1994; Manly,
152 2006) is used to estimate the resulting uncertainties on the hydraulic proper-
153 ties. This method can be used to estimate a statistic without it being biased,
154 to evaluate the accuracy of this estimation and/or to build confidence inter-
155 vals for this statistic. In the present study, the statistics computed are the
156 parameters of the models describing the hydraulic properties. The principle
157 of non-parametric bootstrapping is briefly described below.

158 Let us consider the observation sample obtained for the computation of
159 the statistic, in our case a set of water retention or conductivity measure-
160 ments. These observations must be independent and identically distributed
161 to ensure the convergence of the method. This is the case for almost all
162 configurations in our study and when it is not completely the case (pozzolan
163 and compost conductivity measurements), it has been checked that the pres-
164 ence of dependencies does not significantly influence the results. N artificial
165 samples, of the same size as the original observation sample, are created by
166 sampling in it with replacement. They are called bootstrap samples. The
167 value of the statistic is computed for each one of these bootstrap samples.
168 Its probability distribution is then approximated using the histogram of its
169 N computed values. In other words, the actual variability of the statistic
170 is estimated using the observed variability of all the samples obtained by
171 resampling. In our case, the uncertainty distributions of the estimated hy-
172 draulic properties are thus approximated by fitting the models N times on
173 bootstrap samples of the observations. The number of bootstrap samples
174 used is always set to $N = 500$. It has been verified that the results obtained
175 (mean and standard deviation of the parameters estimated) are stable for

176 this number (variation of only a few percent).

177 Though this methodology does not take into account the problem of
178 model error, of large biases or of samples non representative of the popu-
179 lation, it produces accurate descriptions of uncertainties under reasonable
180 assumptions and a lower bound of the actual uncertainty level. Compared
181 to the maximum likelihood approach, that is classically used for model fit-
182 ting and allows estimating a covariance error matrix for the parameters, the
183 bootstrap approach has the advantage of being free of hypothesis concern-
184 ing the linearity of the model and thus allows estimating non-gaussian error
185 distribution for the parameters. The joint distribution estimated contains
186 the possible dependencies between parameter values resulting from the cal-
187 ibration process. Finally bootstrap method directly gives a sample of this
188 distribution that represents the parameter uncertainties and their depen-
189 dencies. This sample can then easily be used for Monte Carlo uncertainty
190 propagation. The bootstrap method is particularly well suited in our case
191 since numerous replicated observations are available and the models to fit
192 are simple. In case of time-expensive models or numerous parameters, alter-
193 native methods could be used (see for example Brunner et al., 2012).

194 *2.3. Configuration for Richards equation computation*

195 Numerical simulations are performed on a typical soil core to compute the
196 effective parameters at the Darcy scale and to evaluate the reliability of these
197 parameters under dynamic scenarios. In our case, the green roof substrate
198 is represented by a cylinder with the following dimensions: height = 7 cm
199 and diameter = 15 cm. The cylinder is discretized with 507,553 nodes and
200 3,216,152 elements. The average length of each edge is approximately 1.5

201 mm. As mentioned in Appendix A, the pozzolan aggregate size distribution
202 is the following: 2/3 of the pozzolan aggregate diameters ranged from 3 to 6
203 mm, and 1/3 from 7 to 15 mm. A specific algorithm is developed to model
204 the geometry and distribution of pozzolan. This algorithm uses a mesh of
205 the cylinder obtained by GMSH (<http://geuz.org/gmsh/>). Aggregates of
206 pozzolan are then created by randomly selecting a seed represented by an
207 element of the mesh. The volume of the aggregate is randomly chosen from
208 the known aggregate diameter distribution and under the hypothesis that the
209 pozzolan aggregates are spheric. The irregular aggregates are then iteratively
210 built by randomly selecting and aggregating adjacent elements of the growing
211 irregular seeds until the required aggregate volumes are reached. Fig. 2 shows
212 a typical mesh used in the simulations. Initial and boundary conditions are
213 specific to the problem solved (effective parameter computation or evaluation
214 under a dynamic scenario) and are detailed in subsections 2.4 and 2.5.

215 *2.4. Effective parameter computation*

216 The effective parameters are obtained using a steady-state flow simula-
217 tion, as explained in Samouëlian et al. (2007) or Samouëlian et al. (2011).
218 The interval under consideration is $[-10^2, -10^{-2}]$ m, which corresponds to
219 the validity range of the numerical code. The same water matric potential,
220 a Dirichlet type condition, is applied to the upper and the lower boundaries
221 of the cylinder. This leads to a constant water matric potential throughout
222 the medium in the case of homogeneous materials. The vertical boundaries
223 are impermeable. To obtain the hydraulic conductivity, the calculated wa-
224 ter flux is divided by the surface of the upper boundary. In the case of a
225 heterogeneous medium, the same configuration leads to an almost constant

226 water matric potential in the medium, and the so-called effective hydraulic
227 conductivity of the composite substrate is equal to the average water flux
228 density across the horizontal boundaries. The water retention is calculated
229 for each element with a simple arithmetic average. These conductivity and
230 water retention values are relative to the matric potential value set at the
231 boundaries, even if local gradients of matric potential are present within the
232 heterogeneous medium. The computation is thus repeated for several water
233 matric potential values to fit the conductivity and retention curves.

234 To take into account uncertainties in the hydraulic properties of pozzolan
235 and compost, the computation of the effective hydraulic conductivity and
236 water retention for each water matric potential value is repeated for a single
237 set of component properties randomly sampled from their uncertainty distri-
238 butions. The sizes, shapes and spatial distribution of the pozzolan aggregates
239 in the mesh are different for each repetition and are generated randomly as
240 explained in section 2.3. The sampling of pozzolan and compost properties
241 is performed independently for each water matric potential value.

242 The choice of the number and values of water matric potential points,
243 and the number of replicates for each water matric potential value, directly
244 affects the computational cost of the estimation of the effective properties
245 and of their level of uncertainty. An optimal experimental design technique
246 is used to guide these choices. A D-optimal criterion (Atkinson and Donev,
247 1992) is computed to fit the Mualem-van Genuchten and the van Genuchten
248 models. The aim is to minimize the D-criterion, which is the determinant of
249 the error covariance matrices of the models parameters. Several contrasted
250 water matric potential distributions of points are considered in the bounded

251 interval $[-10^2, -10^{-2}]$ m: regular distribution, log-regular distribution and
252 quantiles of beta distributions to concentrate points on the left, the right
253 or the center of the interval. The log-regular distribution appears to be
254 the best compromise with respect to the criterion values computed for both
255 models for a number of water matric potential values. Then, an optimization
256 of the ratio between the number of water matric potential points and the
257 number of replicates, for a given computational cost corresponding to 200
258 simulations, is computed with this log-regular distribution. In the end, the
259 D-optimal design, among those tested, is a log-regular repartition of 4 water
260 matric potential points with 50 replicates. For the Mualem-van Genuchten
261 model fit, prior information from the Wiener bounds on K_{sat} is considered
262 to regularize the fitting problem due to the lack of data at $h = 0$ m.

263 *2.5. Evaluation of the homogenization approach*

264 In order to reduce the impact of non-equilibrium water flow that may
265 appear during dynamic scenarios (Vogel et al., 2008), we use an evaporation
266 scenario to evaluate the homogenization approach because it was noticed that
267 non-equilibrium water flow is more likely to be produced by sharp moisture
268 front obtained during the infiltration process (Roth, 2008). A time-variable
269 flux of evaporation ranging from 1.9 mm d^{-1} to 0.9 mm d^{-1} is applied to the
270 top surface of the soil core at $z = 0$. This evaporation flux is imposed as a
271 Neumann boundary condition at the core surface. The values of the time-
272 variable flux are representative of usual experimental conditions when using
273 the Wind evaporation method. The other boundaries are impermeable. The
274 initial condition is that of a quasi-saturated medium with $h(\mathbf{x}, t = 0) = -9.5$
275 cm for all depths. For $h = -100$ m, the flux type boundary conditions are

276 switched to Dirichlet conditions. The simulations last 10 days to ensure a
277 strong evaporation and a switch from flux to Dirichlet conditions at the upper
278 part of the soil core.

279 200 simulations are performed for the two-component configuration and
280 for the equivalent homogeneous material, by randomly sampling the corre-
281 sponding hydraulic properties in their uncertainty distributions and the sizes,
282 shapes and spatial distribution of the pozzolan aggregates. For each simula-
283 tion, 4 sets of 5 points are considered to monitor the matric potential. They
284 are taken for $z = 0, -0.2, -1.1$ and -4.8 cm, respectively. For each depth,
285 the arithmetic mean values of matric potential are computed on the 5 points.
286 The distribution of these mean values obtained for the two-component con-
287 figuration is then compared to the distribution obtained for the equivalent
288 homogeneous configuration at each depth.

289 **3. Results and Discussion**

290 *3.1. Hydraulic properties and associated uncertainties of individual materials*

291 The water retention measurements of pozzolan are widely spread near
292 saturation (Fig. 3a). High standard deviations for water content, 0.13 m^3
293 m^{-3} to $0.14 \text{ m}^3 \text{ m}^{-3}$, are obtained for matric potential values greater than
294 -10^{-2} m. They decrease to a typical value of $0.03 \text{ m}^3 \text{ m}^{-3}$ in the central part
295 of the water retention curve and are lower than $0.007 \text{ m}^3 \text{ m}^{-3}$ for $h < -10$
296 m. According to the Jurin law, water content near saturation is determined
297 by the proportion of larger pores (up to 1 mm in diameter) that can be
298 found inside the pozzolan aggregates. Due to the small size of the aggregates
299 (diameter of about 5 mm) used in the present study, the proportion of macro

300 pores is highly variable from one aggregate to the other, which explains
301 the high variability of the water content near saturation. For lower matric
302 potential values, the water content variability of pozzolan aggregates may be
303 attributed to factors involved in the pozzolan formation. Indeed, pozzolan
304 is a porous siliceous pyroclastic rock, the porosity of which is created by
305 dissolved gas entrapped in lava during scoria emission. The mineralogy of
306 rocks, the proportion of dissolved gas and the temperature of scoria during
307 volcanic eruption, all affect upon the porosity and pore size distribution of
308 pozzolan rocks.

309 Experimental data are less spread out for the water retention of bark
310 compost (Fig. 3c). Contrary to pozzolan, the water retention measurements
311 for bark compost are obtained on remolded and compacted samples. The
312 porosity of compacted bark compost includes both the matric porosity of
313 individual bark fragments and the structural porosity between bark frag-
314 ments. As observed for natural soils (Dexter et al., 2008), water retention
315 near saturation is linked to the structural porosity. We observe a very good
316 linear relationship between water retention data and apparent bulk density
317 for matric potentials greater than -0.7 m (data not shown). Variability in
318 the water retention measurements is thus very low near saturation, since the
319 apparent bulk density of bark compost samples is accurately controlled. For
320 lower matric potential values, the variability is due to the variability of ma-
321 tric porosity and pore size distribution of bark fragments. This experimental
322 dispersion is relatively low, since the highest standard deviation value is 0.02
323 $\text{m}^3 \text{m}^{-3}$.

324 Figs. 3a and 3c show that the van Genuchten model adequately fits

325 water retention experimental data. Some slight deviations can be found
326 between the mean of the experimental data and the fitted curve for a water
327 potential of about -1 m. However, these deviations are within the range
328 of the experimental dispersion and they do not question the quality of fit.
329 The estimated uncertainty distributions have a similar behavior to those of
330 the experimental ones: a lower level of uncertainty for compost than for
331 pozzolan, particularly for matric potentials between -0.01 m and -1 m,
332 and a higher level of uncertainty near saturation. For both materials, the
333 most variable and least variable parameter, respectively, are h_e and the n
334 exponent, with respective coefficient of variations of approximately 20% and
335 1 % for bark compost data, and 35% and 1 % for pozzolan aggregates data
336 (see Table 1). The h_e parameter is a scale parameter, which is related to
337 the entry point of air into the studied material, whereas parameter n is a
338 shape parameter related to the pore size distribution (Kutilek and Nielsen,
339 1994). A greater scattering of the parameters can thus be linked to the macro
340 porosity variability. A slight variability in exponent n is representative of a
341 homogeneous meso- and micro pore size distribution for both materials.

342 K_{Sat} experimental values range from 10^{-7} to 10^{-3} m.s $^{-1}$ for pozzolan
343 samples (Fig. 3b). The conductivities at saturation of “porous” blocks are
344 higher than those of “dense” blocks (not shown here). The relative standard
345 deviation of K_{Sat} is quite low for compost (Fig. 3d). This is expected as
346 explained in Appendix A. For the unsaturated part of the hydraulic conduc-
347 tivity curve, the scattering of (K, h) experimental data found for pozzolan
348 and bark compost materials are similar to the scattering of data found for
349 natural soils using the Wind evaporation method (Tamari et al., 1993). We

350 observe a lack of experimental values between the data obtained under sat-
351 urated and unsaturated conditions. This is due to the limited accuracy of
352 matric potential sensors and to the Wind evaporation method: it is neces-
353 sary to have significant matric potential gradients between two successive
354 sensors to compute an accurate value of the unsaturated hydraulic conduc-
355 tivity. This is usually not achieved close to saturation (Tamari et al., 1993).
356 Despite this limitation, direct computation of K values can be obtained using
357 the Wind evaporation. This is not the case for inverse methods used either
358 in the one-step or the multi-step outflow methods (Hopmans et al., 2002),
359 where only curve parameters are fitted.

360 Figs. 3b and 3d show that, as expected, the estimated uncertainty of
361 the hydraulic conductivity of pozzolan is greater than that of bark compost.
362 The uncertainty distribution of parameter n is very low for both materials
363 (see Table 2). For the h_e and K_{sat} parameters, the uncertainty is greater for
364 pozzolan material than for bark compost material.

365 *3.2. Effective hydraulic properties and associated uncertainties*

366 The uncertainty distributions of the effective water retention and hy-
367 draulic conductivity values are presented in Figs. 3e and 3f. Estimated
368 values and standard deviations for the corresponding parameters of the van
369 Genuchten and Mualem-van Genuchten models are displayed in Tables 1 and
370 2.

371 The estimated uncertainties for the effective parameters are relatively low
372 and generally lower than those of bark compost and pozzolan under unsat-
373 urated conditions. This is mainly due to the size (number of replicates \times
374 number of water potential values), and to a lower extent, given this size, to

375 the optimal choice of the numerical experimental design used for computing
 376 the effective values. These uncertainties increase close to saturation, follow-
 377 ing the same trend as the one observed for individual components. The stan-
 378 dard deviations of most of the van Genuchten and Mualem-van Genuchten
 379 parameters estimated for the effective material are lower than the ones es-
 380 timated for bark compost and pozzolan. The standard deviations of the
 381 parameters directly linked to saturated conditions (K_{Sat} and θ_s) estimated
 382 for the effective material, are between those estimated for bark compost and
 383 pozzolan.

384 Various analytical bounds or estimations of effective hydraulic conductiv-
 385 ities can be found in the literature (Matheron, 1967; Renard and de Marsily,
 386 1997). The Wiener bounds are the harmonic and arithmetic means of con-
 387 ductivity data and correspond to the effective conductivity of a plane layered
 388 porous medium when the water flux is, respectively, perpendicular or par-
 389 allel to the main orientation of the layered surface. These bounds give a
 390 fundamental inequality which is always valid for complex structure patterns
 391 (Renard and de Marsily, 1997, Samouëlian et al., 2011). Let $\mu_{a|K}$ and $\mu_{h|K}$
 392 be the arithmetic and harmonic means of conductivity values, ω_C and ω_P
 393 the volumetric proportion of each material, and K_C and K_P the hydraulic
 394 conductivities of compost and pozzolan, respectively. For each water matric
 395 potential h , the effective conductivity K_{eff} can be bounded as follows

$$\mu_{h|K} = \frac{1}{\omega_C/K_C + \omega_P/K_P} \leq K_{eff} \leq \mu_{a|K} = \omega_C K_C + \omega_P K_P.$$

396 For a statistically homogeneous and isotropic medium, Matheron (1967)
 397 proposes an estimation of the effective conductivity calculated by a geometric

398 weighted average of the arithmetic and harmonic means $\mu_{a|K}$ and $\mu_{h|K}$. This
399 curve is defined by $\mu_{M|K} = \mu_{a|K}^\alpha \mu_{h|K}^{1-\alpha}$, where $\alpha = (D - 1)/D$ and D is the
400 dimension of the problem.

401 Figs. 4 show the mean and standard deviation of the 50 effective conduc-
402 tivity values at the 4 water matric potential values, as well as the means of
403 the corresponding Wiener bounds and Matheron estimations. The mean of
404 the effective conductivity values, for each water matric potential value, must
405 be included into the mean of the corresponding Wiener bounds. The crosses
406 which can be observed in Figs. 4 are well-bounded, validating the numerical
407 procedure developed to determine the effective values. Note that the mean
408 of the effective conductivity values is closer to the arithmetic mean curve.
409 It is above the Matheron mean curve before the intersection between the
410 Wiener curves, and below after that intersection. Fig. 5 presents the mean
411 and standard deviation of the effective retention values. It is very close to
412 the arithmetic mean curve. This result is already obtained by several authors
413 (Samouëlian et al., 2007; Samouëlian et al., 2011; Vogel et al., 2008 among
414 others). Under quasi-static conditions and without dynamic effects, the wa-
415 ter retention curve presents a capacitive property (Vogel et al., 2008) and
416 the effective water retention curve can be calculated from the additive prop-
417 erties of the local water retention (Samouëlian et al., 2007). The standard
418 deviations of the effective conductivity and retention values computed for
419 the four water potential values are between those obtained for bark compost
420 and pozzolan, and close to the standard deviation of their arithmetic mean
421 (results not shown).

422 In summary, the methodology using an optimal sampling design leads

423 to “well defined” effective properties. We show that the uncertainties of
424 the effective properties are lower than the uncertainties of the properties of
425 each material. The reduction in the level of uncertainty is more pronounced
426 for the van Genuchten parameters associated to the dry part of the proper-
427 ties (θ_r, h_e, n) than for the ones associated to the wet part of the properties
428 (θ_s, K_{sat}) .

429 *3.3. Evaluation of the homogenization approach under dynamic evaporation*

430 Three snapshots of water potential values obtained during the evapora-
431 tion process are presented in Figs. 6 for the two-component configuration.
432 Heterogeneous spatial distributions of these values are observed at the upper
433 surface of the soil core at $t = 2$ days and $t = 6$ days. Blue shades represent
434 the gradients due to the geometrical distribution of the two materials. Con-
435 sequently, isovalues of h do not correspond to horizontal planes. At $t = 10$
436 days, the Dirichlet condition replaces the flux condition at the upper surface,
437 which leads to a uniform spatial distribution of water matric potential values
438 at $z = 0$. A gradually stronger vertical gradient could be seen in-depth as
439 evaporation takes place.

440 Figs. 7 present the uncertainty distributions of water matric potential
441 mean values per depth for the two-component configuration and the cor-
442 responding effective homogeneous material configuration. The uncertainty
443 distributions obtained for the effective homogeneous material configuration
444 are clearly less scattered than those obtained for the two-component config-
445 uration, and are included in their [25th, 75th] percentile ranges (not shown
446 here). This is a direct consequence of the lower level of uncertainties of the
447 effective hydraulic properties compared to those of compost and pozzolan.

448 Note however that the level of uncertainty obtained here for the simulation
449 of water matric potential might not be representative of the level of uncer-
450 tainty expected on the simulation of a real evaporation experiment. In this
451 last case, other types of uncertainties, such as uncertainties on initial and
452 boundary conditions for example, must be taken into account.

453 The mean of these uncertainty distributions for each simulation configu-
454 ration and depth is also presented in Figs. 7. The curves obtained for the
455 effective homogeneous material and the explicit two-component medium are
456 similar. This confirms the validity of our approach. However, some discrep-
457 ancies appear as simulation time increases. Table 3 shows the mean water
458 matric potential values and the mean water content values for both configu-
459 rations at $t_{max} = 10$ days, the final time point of the evaporation simulation.
460 Relative differences between the two configurations are quite high for water
461 matric potentials, and are more pronounced in-depth. However, these relative
462 differences correspond to an area of the core where the porous media are dry.
463 Water content values of both the two-component and the homogeneous ma-
464 terial configurations are computed from these water matric potentials using
465 the van Genuchten model and the parameters estimated for the effective ma-
466 terial configuration given in Table 1. These water content values presented in
467 Table 3 show only slight differences between the two configurations, and the
468 relative differences (between 2.1% and 6.4% at 10 days) are lower than those
469 of the water matric potentials. Note that these discrepancies may be due to
470 the non-equilibrium flow process, a consequence of the occurrence of tran-
471 sient processes during the dynamic simulation. This point has been showed
472 theoretically by Lewandowska et al. (2004) in the framework of the homoge-

473 nization theory : a sink-source term accounting for non-equilibrium processes
474 is added to the Richards equation during the upscaling process. However,
475 this non-equilibrium water flow should be minimized under evaporation sce-
476 narios compared to infiltration scenarios because of smoother moisture front
477 (Roth, 2008). Moreover, results obtained by Simunek et al. (2001) show
478 that modeling a non-equilibrium flow modifies the dynamic response for in-
479 filtration scenarios, but hardly affects the dynamic response for evaporation
480 scenarios. During the evaporation simulation, the average macroscopic flux
481 is a vertical upward flux. However, the orientation of the local, microscopic
482 water flux could be derived from the vertical direction, due to the presence
483 of local heterogeneous water potential gradients as shown in Figs. 6. The
484 tortuosity of the water flow is, thus, increased. This local tortuosity is a kind
485 of balance between the boundary conditions leading to a vertical macroscopic
486 flux and the contrast of the hydraulic properties of both materials leading to
487 the multidimensional microscopic water flux. The contrast of the hydraulic
488 properties depends on the local water content or matric potentials, and as
489 these variables are time dependent during the dynamic simulation, the tortu-
490 osity is also time dependent. This time-dependent tortuosity is not accounted
491 for during the upscaling process since the determination of the effective prop-
492 erties is performed under successive states of equilibrium. Consequently to
493 the time dependency of the local tortuosity, the overall evaporation process
494 of the heterogeneous medium could be accelerated or slowed down compared
495 to the effective material. Therefore, more complex models including non-
496 equilibrium terms might be implemented to study their influence on the
497 dynamic response using the present configuration.

498 4. Conclusion

499 The hydraulic properties of a heterogeneous medium are studied at the
500 Darcy scale using two different approaches. The first approach consists in
501 determining the water retention and hydraulic conductivity curves for the
502 components of the heterogeneous medium. The material considered herein is
503 a green roof substrate, which is a composite of compressible materials, bark
504 compost, and of aggregates of volcanic rock, pozzolan. Associated uncer-
505 tainties are evaluated using a bootstrap method. It is shown, on a virtual
506 evaporation experiment, that the impact of these uncertainties on the simu-
507 lated water matric potential is high.

508 The second approach considers the heterogeneous medium as an homoge-
509 neous material. Effective water retention and hydraulic conductivity curves
510 are fitted on values computed for several water matric potentials using nu-
511 merical steady-state scenarios on the heterogeneous material. Associated
512 uncertainties of these properties are also evaluated, considering the uncer-
513 tainties of the hydraulic properties of each component. As far as we know,
514 this is the first time uncertainty analysis is performed for the computation
515 of effective properties. To that effect, for each hydraulic property, N couples
516 of curves are sampled in the uncertainty distributions of the components in
517 an independent way for a set of water matric potential values. N is set at a
518 high value, and the water matric potential values are optimally chosen. We
519 show that this methodology leads to very low levels of uncertainties in the
520 effective properties of the material. Despite high level of uncertainties on the
521 hydraulic parameters of the two-component material, effective properties of
522 the heterogeneous media can thus be precisely defined using the bootstrap

523 method. A direct consequence is that the uncertainties of simulated water
524 potential for the effective material are very low compared to those obtained
525 on the heterogeneous medium. Nevertheless, their mean values are almost
526 similar for dynamic evaporation which confirms the relevance of the approach
527 in these conditions.

528 Our work shows thus that when non-equilibrium water flow can be ne-
529 glected, it is preferable to work with the effective parameters rather than with
530 the heterogeneous and distributed parameters in order to reduce uncertain-
531 ties on the water balance. This is of importance since the uncertainties linked
532 to the experimental setup and to the variability of the materials properties
533 may be high, as shown in the first part of the study.

534 Simulation models which include a non-equilibrium term could be used in
535 the scope of future studies to evaluate the relevance of effective parameters
536 and the impact of their uncertainties in a larger range of conditions.

537 **Acknowledgment**

538 This work was supported by the French National Research Agency (ANR)
539 through the “Habitat intelligent et solaire photovoltaïque” program (project
540 AGROBAT ANR-09-HABISOL-001). We also thank the CINES (Centre
541 Informatique National de l’Enseignement Supérieur, France) for offering us
542 access to the supercomputer JADE to conduct these calculations successfully.
543 The authors wish to thank Profs. L. Di Pietro, G. Micolau, H. Bolvin and Dr.
544 C. Doussan for their helpful comments and careful readings of the manuscript.

- 545 Atkinson, A.C., Donev, A.N., 1992. Optimum Experimental Designs, vol-
546 ume 8 of Oxford Statistical Science Series, 1st edn. Oxford University Press,
547 Oxford, UK, 352pp.
- 548 Bechtold, M., Vanderborght, J., Weihermuller, L., Herbst, M., Gunther,
549 T., Ippisch, O., Kasteel, R., Vereecken, H., 2012. Upward transport in a
550 three-dimensional heterogeneous laboratory soil under evaporation condi-
551 tions. *Vadose Zone J.* 11(2).
- 552 Besson, A., Cousin, I., Samouëlian, Boizard, H., Richard, G., 2004. Struc-
553 tural heterogeneity of the soil tilled layer as characterized by 2D electrical
554 resistivity surveying, *Soil & Tillage Res.* 79, 239–249.
- 555 Bierkens, M.F.P., van der Gaast, J.W.J., 1998. Upscaling hydraulic con-
556 ductivity: theory and examples from geohydrological studies. *Nutri. Cycl.*
557 *Agroecosyst.* 50, 193–207.
- 558 Brunner, P., Doherty, J., Simmons, C.T., 2012. Uncertainty assessment and
559 implications for data acquisition in support of integrated hydrologic models.
560 *Water Resour. Res.* 48(7).
- 561 Carter, T., Jackson, C.R., 2007. Vegetated roofs for stormwater manage-
562 ment at multiple spatial scales. *Landsc. Urban Plan.* 80, 84–94.
- 563 Celia, M.A., Bouloutas, E.T., Zarba, R.L., 1990. A general mass-
564 conservative numerical solution for the unsaturated flow equation. *Water*
565 *Resour. Res.* 26(7), 1483–1496.
- 566 Chossat, J.C., 2005. La mesure de la conductivité hydraulique dans les sols

567 - Choix des méthodes, 1st edn. Tec et Doc - Lavoisier Editions, London,
568 Paris, New York, 720pp.

569 Christiaens, K., Feyen, J., 2001. Analysis of uncertainties associated with
570 different methods to determine soil hydraulic properties and their propaga-
571 tion in the distributed hydrological MIKE SHE model. *J. Hydrol.* 246(1-4),
572 63–81.

573 Coleman, T.F., Li, Y., 1996. An Interior, Trust Region Approach for Non-
574 linear Minimization Subject to Bounds. *SIAM J. Optimiz.* 6(2), 418–445.

575 Coppola, A., Basile, A., Comegna, A., Lamaddalena, N., 2009. Monte Carlo
576 analysis of field water flow comparing uni- and bimodal effective hydraulic
577 parameters for structured soil. *J. Contam. Hydrol.* 104(1-4), 153–165.

578 Dane, J.H., Hopmans, J.W., 2002. Methods of soil analysis: Part 4 Physical
579 methods, In: Dane, J.H., Topp, G.C. and Campbell, G.S. (Ed.) *Soil Science*
580 *Society of America, Madison:SSSA book series 5*, 1662pp.

581 Danquigny, C., Ackerer, P., 2005. Experimental determination of equivalent
582 parameters of a heterogeneous porous medium under uniform or radial flow.
583 *C. R. Geoscience.* 337(6), 563–570.

584 Dexter, A.R., Czyz, E.A., Richard, G., Reszkowska, A., 2008. A user-
585 friendly water retention function that takes account of the textural and
586 structural pore spaces in soil. *Geoderma.* 143(3-4), 243–253.

587 Dhatt, G., Touzot, G., Lefrançois, E., 2007. *Méthode des éléments finis*, 4th
588 edn. *Hermes Science Publications - Lavoisier Editions*, London, Paris, New
589 York, 601pp.

- 590 Dulu, O.G., 1999. Computer axial tomography in geosciences : an
591 overview. *Earth-Sci. Rev.* 48, 265–281.
- 592 Efron, B., Tibshirani, R., 1994. An Introduction to the Bootstrap, Mono-
593 graphs on Statistics & Applied Probability (Book 57), 1st edn. Chapman
594 & Hall/CRC, London, UK, 456pp.
- 595 Fityus, S.G., Smith, D.W., 2001. Solution of the unsaturated soil mois-
596 ture equation using repeated transforms. *Int. J. Numer. Anal. Methods*
597 *Geomech.* 25(15), 1501–1524.
- 598 Forschungsgesellschaft Landschaftsentwicklung Landschaftsbau e.V.–FLL,
599 2002. Guidelines for the planning, execution and upkeep of green-roof
600 sites, 1st edn. Forschungsgesellschaft Landschaftsentwicklung Landschafts-
601 bau e. V. - FLL, Bonn, Germany, 97 pp. URL: <http://www.fll.de>
- 602 Hardelauf, H., Javaux, M., Herbst, M., Gottschalk, S., Kasteel, R., Van-
603 derborght, J., Vereecken, H., 2007. PARSWMS: A parallelized model for
604 simulating three-dimensional water flow and solute transport in variably
605 saturated soils. *Vadose Zone J.* 6(2), 255–259.
- 606 Herbst, M., Gottschalk, S., Reissel, M., Hardelauf, H., Kasteel, R., Javaux,
607 M., Vanderborght, J., Vereecken, H., 2008. On preconditioning for a parallel
608 solution of the Richards equation. *Comput. & Geosci.* 34(12), 1958–1963.
- 609 Hopmans, J.W., Šimůnek, J., Romane, N., Durner, W., 2002. Methods of
610 Soil analysis - Part 4 Physical Methods, In: Dane, J.H., Topp, G.C. and
611 Campbell, G.S. (Ed.) Soil Science Society of America, Madison:SSSA book
612 series 5, 1662pp.

- 613 Huang, K., Mohanty, B.P., van Genuchten, Mth., 1996. A new convergence
614 criterion for the modified Picard iteration method to solve the variably
615 saturated flow equation. *J. Hydrol.* 178(1-4), 69–91.
- 616 Javaux, M., Vanclooster, M., 2006a. Three-dimensional structure character-
617 isation and transient flow modelling of a variably saturated heterogeneous
618 monolith. *J. Hydrol.* 327(3-4), 516–524.
- 619 Javaux, M., M. Vanclooster, M., 2006b. Scale-dependency of the hydraulic
620 properties of a variably saturated heterogeneous sandy subsoil. *J. Hydrol.*
621 327, 376–388.
- 622 Ju, S.H., Kung, K.J.S., 1997. Mass types, element orders and solution
623 schemes for the Richards equation. *Comput. & Geosci.* 23(2) 175–187.
- 624 Kavetski, D., Binning, P., Sloan, S.W., 2001. Adaptive time stepping and
625 error control in a mass conservative numerical solution of the mixed form
626 of Richards equation. *Adv. Water Resour.* 24(6), 595–605.
- 627 Khaleel, R., Yeh, T.C.J., Lu, Z., 2002. Upscaled flow and transport proper-
628 ties for heterogeneous unsaturated media, *Water Resour. Res.* 38, 1053.
- 629 Kutilek, M., Nielsen, D.R., 1994. *Soil Hydrology*, 1st edn. Catena Verlag
630 GMBH, Reiskirchen, Germany, 370pp.
- 631 Lewandowska, J., Szymkiewicz, A., Burzynski, K., Vauclin, M., 2004. Mod-
632 eling of unsaturated water flow in double-porosity soils by the homogeniza-
633 tion approach. *Adv. Water Resour.* 27, 283–296.

- 634 Ma, D., Shao, M., Zhang, J., Wang, Q., 2010. Validation of an analytical
635 cal method for determining soil hydraulic properties of stony soils using
636 experimental data. *Geoderma*. 159, 262–269.
- 637 Manly, B.F.J., 2006. *Randomization, Bootstrap and Monte Carlo Methods*
638 *in Biology*, 3rd edn. Chapman & Hall/CRC, London, UK, 480pp.
- 639 Mantoglou, A., Gelhar, L.W., 1987. Stochastic modeling of large-scale tran-
640 sient unsaturated flow flow systems. *Water Resour. Res.* 23, 37–46.
- 641 Matheron G., 1967. *Eléments pour une Théorie des Milieux Poreux*, 1st
642 edn. Masson et Cie, Paris, France, 168pp.
- 643 Mohrath, D., Bruckler, L., Bertuzzi, P., Gaudu, J.C., Bourlet, M., 1997.
644 Error analysis of an evaporation method for determining hydrodynamic
645 properties in unsaturated soil. *Soil Sci. Soc. Am. J.* 61(3), 725–735.
- 646 Monnier, G., Stengel, P., Fiès, J.C., 1973. Une méthode de mesure de la
647 densité apparente de petits agglomérats terreux. Application à l’analyse des
648 systèmes de porosité du sol. *Ann. agron.* 24(5), pp. 533-545.
- 649 Ouldboukhitine, S.E., Belarbi, R., Djedjig, R., 2012. Characterization of
650 green roof components: Measurements of thermal and hydrological proper-
651 ties. *Build Environ.* 56, 78–85.
- 652 Pan, F., Ye, M., Zhu, J., Wu, Y.S., Hu, B.X., Yu, Z., 2009. Numerical eval-
653 uation of uncertainty in water retention parameters and effect on predictive
654 uncertainty. *Vadose Zone J.* 8(1), 158–166.

- 655 Peters, A., Durner, W., 2008. Simplified evaporation method for determin-
656 ing soil hydraulic properties. *J. Hydrol.* 356(1-2), 147–162.
- 657 Renard, Ph., de Marsily, G., 1997. Calculating equivalent permeability: a
658 review. *Adv. Water Resour.* 20(5-6), 253–278.
- 659 Renaud, J., Cloke, H., Wang, Y., Anderson, M., Wilkinson, P., Lloyd, D.,
660 2003. Simulation numérique d'écoulements en milieu poreux avec l'équation
661 de Richards. *Eur. J. Comput. Mech.* 12(2-3), 203–220.
- 662 Roth, K., 2008. Scaling of water flow through porous media and soils. *Eur.*
663 *J. of Soil Sci.* 59, 125–130.
- 664 Russo, D., 1992. Upscaling of hydraulic conductivity in partially saturated
665 heterogeneous porous formation. *Water Resour. Res.* 28, 397–409.
- 666 Samouëlian, A., Vogel, H.J., Ippisch, O., 2007. Upscaling hydraulic conduc-
667 tivity based on the topology of the sub-scale structure. *Adv. Water Resour.*
668 30(5), 1179–1189.
- 669 Samouëlian, A., Cousin, I., Dagès, C., Frison, A., Richard, G., 2011. De-
670 termining the effective hydraulic properties of a highly heterogeneous soil
671 horizon. *Vadose Zone J.* 10(1), 450–458.
- 672 Simunek J., Wendroth, O., Wypler, N., van Genuchten, M.Th., 2001. Non-
673 equilibrium water flow characterized by means of upward infiltration exper-
674 iments. *Eur. J. Soil. Sci.* 52(1), 13–24.
- 675 Tabbagh, A., Dabas, M., Hesse, A., Panissod, C., 2000. Soil resistivity: a
676 non-invasive tool to map soil structure horization. *Geoderma* 97, 393–404.

- 677 Tamari, S., Bruckler, L., Halbertsma, J., Chadoeuf, J., 1993. A simple
678 method for determining soil hydraulic properties in the laboratory. *Soil Sci.*
679 *Soc. Am. J.* 57(3), 642–651.
- 680 Tracy, F.T., 2007. Three-dimensional analytical solutions of Richards' equa-
681 tion for a box-shaped soil sample with piecewise-constant head boundary
682 conditions on the top. *J. Hydrol.* 336(3-4), 391–400.
- 683 Vanderborght, J., Kasteel, R., Herbst, M., Javaux, M., Thiéry, D., Van-
684 clooster, M., Mouvet, C., Vereecken, H., 2005. A set of analytical bench-
685 marks to test numerical models of flow and transport in soils. *Vadose Zone*
686 *J.* 4(1), 206–221.
- 687 van Genuchten, MTh., 1980. A closed-form equation for predicting the hy-
688 draulic conductivity of unsaturated soils. *Soil Sci. Soc. Am. J.* 44(5), 892–
689 898.
- 690 Vereecken, H., Kasteel, R., Vanderborght, J., Harter, T., 2007. Upscaling
691 hydraulic properties and soil water flow processes in heterogeneous soils: a
692 review. *Vadose Zone J.* 6, 1–28.
- 693 Vogel, H.J., Roth, K., 1998. A new approach for determining soil hydraulic
694 functions. *Eur. J. Soil Sci.* 49(4), 547–556.
- 695 Vogel, H.J., Samouëlian, A., Ippisch, O., 2008. Multi-step and two-step
696 experiments in heterogeneous porous media to evaluate the relevance of
697 dynamic effectes. *Adv. Water Resour.* 31(1), 181–188.
- 698 Vogel, H.J., Weller, U., Ippisch, O., 2010. Non-equilibrium in soil hydraulic
699 modelling. *J. Hydrol.* 393(1-2), 20–28.

- 700 Wildenschild, D., Jensen, K.H., 1999a. Laboratory investigations of effective
701 flow behavior in unsaturated heterogeneous sands. *Water Resour. Res.* 35,
702 17–27.
- 703 Wildenschild, D., Jensen, K.H., 1999b. Numerical modeling of observed
704 effective flow behavior in unsaturated heterogeneous sands. *Water Resour.*
705 *Res.* 35, 29–42.
- 706 Yang, J., Yu, Q., Gong, P., 2008. Quantifying air pollution removal by
707 greenroofs in Chicago. *Atmos. Environ.* 42, 7266–7273.
- 708 Yeah, T.C.J., Gelhar, L.W., Gutjahr, A.L., 1985. Stochastic analysis of un-
709 saturated flow in heterogeneous soils. 1. Statistically isotropic media. *Water*
710 *Resour. Res.* 21, 447–456.
- 711 Zhang, Y., Gable, C.W., Sheets, B., 2010. Equivalent hydraulic conductivity
712 of three-dimensional heterogeneous porous media: An upscaling study based
713 on an experimental stratigraphy. *J. Hydrol.* 388, 304–320.

		θ_r $\text{m}^3 \text{ m}^{-3}$	θ_s $\text{m}^3 \text{ m}^{-3}$	$ h_e $ m	n
Compost	Estimat. value	$8.66e^{-2}$	$5.55e^{-1}$	$7.47e^{-3}$	1.22
	σ	$5.92e^{-3}$ (6.9%)	$1.27e^{-2}$ (2.3%)	$1.63e^{-3}$ (21.8%)	$1.01e^{-2}$ (0.8%)
Pozzolan	Estimat. value	$0(\text{fixed})$	$3.53e^{-1}$	$5.88e^{-3}$	1.29
	σ	$0(\text{fixed})$	$1.63e^{-2}$ (4.6%)	$2.05e^{-3}$ (34.9%)	$1.11e^{-2}$ (0.9%)
Effective material	Estimat. value	$3.81e^{-2}$	$4.35e^{-1}$	$6.71e^{-3}$	1.26
	σ	$7.17e^{-4}$ (1.9%)	$1.36e^{-2}$ (3.1%)	$1.04e^{-3}$ (15.5%)	$2.74e^{-3}$ (0.2%)

Table 1: Estimated values and associated uncertainties of the van Genuchten model parameters for water retention of compost, pozzolan and effective material.

		K_{Sat} m.s ⁻¹	$ h_e $ m	n
Compost	Estimat. value	$3.04e^{-3}$	$9.72e^{-3}$	1.12
	σ	$1.03e^{-4}$ (3.4%)	$2.79e^{-4}$ (2.9%)	$8.87e^{-3}$ (0.8%)
Pozzolan	Estimat. value	$6.94e^{-6}$	$6.01e^{-1}$	1.02
	σ	$7.95e^{-6}$ (114.6%)	$9.90e^{-1}$ (164.7%)	$9.64e^{-3}$ (0.9%)
Effective material	Estimat. value	$9.36e^{-4}$	$2.28e^{-2}$	1.05
	σ	$8.91e^{-5}$ (9.5%)	$8.01e^{-4}$ (3.5%)	$1.91e^{-3}$ (0.2%)

Table 2: Estimated values and associated uncertainties of the Mualem-van Genuchten model parameters for hydraulic conductivity of compost, pozzolan and effective material.

		Depth= -0.2 cm	Depth= -1.1 cm	Depth= -4.8 cm
Water matric potential means (m)	Effective homogeneous material configuration	-45.78	-15.33	-5.68
	Two-component configuration	-53.71	-21.47	-8.36
	Relative differences	14.8%	28.6%	32.1%
Water content means (m.m ⁻³)	Effective homogeneous material configuration	7.81 e-2	9.12 e-2	10.69 e-2
	Two-component configuration	7.65 e-2	8.68 e-2	10.00 e-2
	Relative differences	2.1%	4.9%	6.4%

Table 3: Means of all water matric potential and water content values for several depth and for the two-component and effective material configurations.

714 **Appendix A. Experimental procedures**

715 The green roof substrate under study is composed of a combination of 40%
716 organic material (bark compost) and 60% volcanic material (pozzolan). This
717 combination corresponds to the volumetric proportions which are actually
718 used in in situ environments.

719 *Determination of solid density and apparent bulk density of compost and* 720 *pozzolan*

721 Pozzolan materials are extracted in a quarry located in the “Massif Cen-
722 tral” mountain, in the center of France. Chemical composition of pozzolan is
723 given by the operator of the quarry (SiO_2 : 42–55%; Al_2O_3 : 12–24%; Fe_2O_3 :
724 8 – 20%). The pozzolan aggregate size distribution is the following: 2/3 of
725 the pozzolan aggregate diameters ranged from 3 to 6 mm, and 1/3 from 7 to
726 15 mm. Bark compost is provided by an industrial partner and the precise
727 composition of this compost is confidential.

728 The properties of the two materials are measured on samples of both
729 materials, and are measured at the same bulk density [ML^{-3}] as they occur
730 in the actual substrate.

731 Samples are crunched, sieved at 315 μm and air dried in the oven for 24 h
732 at 105 °C. Solid particles are then placed in the measurement chamber of a He
733 pycnometer and solid bulk density is determined using the Boyle law (Dane
734 and Hopmans, 2002). The apparent bulk density of pozzolan aggregates is
735 measured on replicates with diameters varying from 7 to 15 mm, using the
736 Archimede law and buoyancy measurements in water. The aggregates are
737 previously saturated in water for 24 h (Monnier et al., 1973). The apparent

738 bulk density of the composite substrate is measured using the core method
739 (Dane and Hopmans, 2002) adapted for compacted and remolded samples.

740 Since bark compost is a compressible material, contrary to pozzolan, we
741 follow the procedure described hereafter to be sure that the density of pure
742 bark compost samples is the same as the density of bark compost present in
743 the actual composite substrate: the complex substrate is characterized fol-
744 lowing a standard compaction methodology, namely the Proctor compaction
745 test, standard DIN 18127. The sample is struck 6 times by a 4.5 kg Proctor
746 hammer from a height of 45 cm to obtain adequate compaction. The com-
747 pacted sample obtained following this methodology is supposed to be repre-
748 sentative of the in situ industrial execution of the green roofs (Forschungs-
749 gesellschaft Landschaftsentwicklung Landschaftsbau e. V. - FLL, 2002). By
750 knowing, on the one hand, the apparent bulk density of the substrate and
751 of the pozzolan aggregates and, on the other hand, the solid density of bark
752 compost and of pozzolan, we extrapolate the apparent bulk density of bark
753 compost in the actual composite substrate.

754 All the measured properties are displayed in Table A.4.

755 *Determination of water retention and associated uncertainties*

756 Water retention measurements are obtained using the suction table for
757 small suctions (0.05, 0.54, 1.03, 2.01, 3.97, 6.91 kPa) and the pressure plate
758 extractors for large suctions (10, 30, 50, 100, 300, 500 and 1500 kPa) (Dane
759 and Hopmans, 2002). The total number of replicates differs for pozzolan and
760 bark compost materials.

- 761 1. Since pozzolan aggregates are a natural material with a high level of
762 variability due to geological variations occurring during their formation,

		Pozzolan ag- gregate	Complex substrate	Bark com- post
Particle density (kg.m^{-3})	Mean	3.000	-	1.670
	σ coefficient of variation	0.020 0.7%	- -	0.040 2.4%
Apparent bulk density (kg.m^{-3})	Mean	1.520	0.822	0.195
	σ coefficient of variation	0.230 15.1%	0.002 0.2%	0.003 1.5%

Table A.4: Mean and standard deviation values of the particle and apparent bulk densities for bark compost, pozzolan aggregate and complex substrate.

763 a large number of replicates are required to counter the effects of this
764 natural heterogeneity. 10 different aggregates are used for each suction
765 point. The aggregates taken for apparent bulk density measurements
766 are also used for the 0 kPa suction point. Water saturated aggregates
767 are gently placed onto a fine layer of kaolinite paste to ensure a good
768 contact between aggregate pores and the sand layer (for suction tables)
769 or the porous plate (for pressure plate extractors). A set time for sample
770 equilibration of 3 days is respected.

771 2. Bark compost samples are compacted in the laboratory following a
772 standard procedure to obtain a predetermined density of compost into
773 the composite substrate, the variability of which is very low (see Table
774 A.4). A low number of replicates are, therefore, required. 5 different
775 bark compost samples are used for each suction point. To account
776 for any natural variability in the density of bark compost within the
777 composite substrate, samples are compacted in small cylinders ranging
778 from 0.184 and 0.213 g.cm⁻³. Mean bulk density is 0.200 g.cm⁻³, which
779 differs slightly from the theoretical bulk density of compost within the
780 composite substrate (0.195 g.cm⁻³), due probably to experimental ap-
781 proximations. After initial saturation, samples are placed onto the
782 suction table or porous plate. Kaolinite paste is also used to increase
783 the quality of the capillary connectivity between the sample and the
784 sand layer or porous plate. The time needed for sample equilibrium is
785 over one week for each suction point and is controlled by monitoring
786 the water flow out of the pressure chamber.

787 *Determination of hydraulic conductivity and associated uncertainties*

788 Hydraulic conductivity is measured for pozzolan and bark compost un-
789 der water-saturated and unsaturated conditions using two different meth-
790 ods. Hydraulic conductivity at saturation K_{Sat} [LT^{-1}] is measured using
791 a constant head permeameter (Chossat, 2005) for pozzolan cores and bark
792 compost samples. Unsaturated hydraulic conductivity is measured using the
793 Wind evaporation method (Tamari et al., 1993). Samples used for determin-
794 ing the hydraulic conductivity at saturation are also used to determine the
795 unsaturated hydraulic conductivities. As is the case of the water retention
796 curve, the number of replicates differs for pozzolan and bark compost, and is
797 adapted to the different variability of both materials: 10 replicates are used
798 for pozzolan and 1 replicate is used for bark compost.

799 Samples of pozzolan are extracted from large blocks (volume of approxi-
800 mately 1 dm^{-3}). A classification of these blocks is initially made based on the
801 visible porosity and the estimated bulk density: an equal number of “com-
802 pact” and “porous” blocks in equal quantities are identified. 10 replicates
803 are then cored from both types of blocks. The vertical walls of the clods are
804 surrounded by heat shrink tubing to avoid preferential water flow along the
805 walls during measurements. The uncertainty distribution of the measured
806 hydraulic conductivity at saturation used in section 3.1 is estimated as the
807 experimental variability of K_{Sat} measurements.

Samples of bark compost are obtained after their compaction up to 0.195 g.cm^{-3} in cylinders. A single replicate is used, since a low experimental variability is expected as the compaction procedure is accurately performed and leads to a very low level of variability in the porosity obtained (see

Table A.4). Porosity ϕ of bark compost is measured for this single sample. The uncertainty of the measured saturated hydraulic conductivity could thus be estimated from the variability in the porosity values using the Kozeny-Carman model (Kutilek and Nielsen, 1994). A simple error propagation computed using this model, assuming a log-normal distribution of K_{Sat} , gives rise to

$$\text{var} [\log(K_{Sat})] = \left(\frac{3 - \phi}{\phi(1 - \phi)} \right)^2 \text{var}(\phi).$$

808 For measuring the unsaturated hydraulic conductivity, pozzolan clods and
 809 bark compost are equipped with sufficient microtensiometers to obtain an
 810 accurate estimation of their hydraulic properties (Tamari et al., 1993). After
 811 the sample saturation, water is allowed to evaporate from the upper surface
 812 of each core under laboratory conditions, i.e. conditioned atmosphere at 24
 813 °C under atmospheric pressure. The base of each core is sealed to prevent
 814 downward flux.

815 **Appendix B. C++ parallelized code**

816 The three-dimensional variably saturated flow modeling is based on the
 817 non-linear Richards equation. The mixed form of Richards equation obtained
 818 by combining the mass conservation law with the generalized Darcy equation
 819 is

$$\frac{\partial \theta(h, \mathbf{x}, t)}{\partial t} = \nabla \cdot (K(h, \mathbf{x}, t) \nabla (h(\mathbf{x}, t) + z)) \quad (\text{B.1})$$

820 where z is the upward vertical coordinate. Constitutive functions depending
 821 on the materials considered link $h(\mathbf{x}, t)$, $\theta(h, \mathbf{x}, t)$ and $K(h, \mathbf{x}, t)$ and close
 822 (B.1). Various initial and boundary conditions can complete the parabolic
 823 system of partial differential equations.

824 Water flow is solved using the mixed form of the Richards equation, for
825 which a perfect mass balance is ensured (Celia et al., 1990; Kavetski et al.,
826 2001; Renaud et al., 2003 to cite a few). Spatial discretization is performed
827 using the Galerkin-type linear isoparametric finite elements (Dhatt et al.,
828 1984; Ju and Kung, 1997). The modified Picard iteration scheme is imple-
829 mented in a fully implicit Euler time discretization. Different convergence
830 criterion can be used, as explained in Huang et al. (1996). An adaptive time
831 step adjustment is implemented to improve numerical efficiency (Kavetski et
832 al., 2001). Time and spatial discretizations result in the following system of
833 linear equations

$$\left[\frac{[M^{t+1,m}][C^{t+1,m}]}{\Delta t} + [K^{t+1,m}] \right] \{\delta_u^m\} =$$

$$\{F^{t+1,m}\} - \frac{[M^{t+1,m}]}{\Delta t} \{\theta^{t+1,m}\} + \frac{[M^{t+1,m}]}{\Delta t} \{\theta^t\} - [K^{t+1,m}] \{u^{t+1,m}\} \quad \text{(B.2)}$$

834 where t and m denote, respectively, time and inner iteration levels, $u = h + z$
835 and $\delta_u^m = u^{t+1,m+1} - u^{t+1,m}$, $[M]$ and $[K]$ are the global mass and stiffness
836 matrices, F includes the source/sink terms and $[C(h, \mathbf{x}, t)]$ is the specific
837 moisture capacity function matrix.

838 A C++ object oriented code (FAFEMO) has been developed to solve
839 (B.2) and to determine the water matric potential and the water flux at each
840 node/boundary of the finite element mesh grid for an unsaturated medium.
841 Our numerical results are found to corroborate analytical results published by
842 Tracy (2007), Fityus and Smith (2001) or purely numerical results proposed
843 by Vanderborgh et al. (2005).

844 Due to the specific composition of the green roof substrate, very fine spa-
845 tial grids are required, leading to huge CPU time and storage cost. This

846 major drawback is overcome by a parallelization of code FAFEMO with
847 a similar parallelization strategy as the one presented in Hardelauf et al.,
848 2007, or Herbst et al., 2008. MPI (<http://www.mpi-forum.org/>) and PETSc
849 (<http://www.mcs.anl.gov/petsc/>) libraries were used herein to parallelize the
850 C++ sequential code.

LaTeX Source Files

[Click here to download LaTeX Source Files: JH_V27_unmarked.tex](#)

Highlights:

- The effective hydraulic properties of real heterogeneous media were evaluated at the Darcy scale.
- The suitability of the homogenization approach was shown in a case of dynamic evaporation simulations.
- We accounted for the uncertainties for the hydraulic properties of each material.
- A reduction in the level of uncertainties was obtained for the effective hydraulic properties.

List of captions

Figure 1:

General flowchart of the approach. # is used to symbolise several samples or values. Blue color is used for the description of the processing of the heterogeneous material and its individual components, green color for the effective material, red color for the treatment of uncertainties.

Figure 2:

Typical heterogeneous mesh for the two-component configuration. Black or white zones correspond, respectively, to the pozzolan or bark compost components.

Figure 3:

Uncertainty distributions of a) pozzolan, c) compost and e) effective water retention values. Crosses and error bars represent means and ± 1 standard deviations of measured or simulated data and curves represent 0.5, 2.5, 25, 75, 97.5, 99.5 percentiles and median of the estimated water retention uncertainty distributions. Vertical axes are in log scale. Uncertainty distributions of b) pozzolan, d) compost and f) effective hydraulic conductivity values. Data obtained for pozzolan samples are represented with the same symbol since experimental scattering largely overlaps from one sample to the other. Vertical and horizontal axes are in log scale. Water potential axes are cut to artificially plot asymptotic behaviour and measured values at 0 m in log scale.

Figure 4:

Effective conductivity values computed from 200 compost and pozzolan properties for 4 water matric potential values. Crosses represent the mean and ± 1 standard deviations of the 50 computed values per water matric potential point, dotted lines are the means of the Wiener bounds and the plain line is the Matheron curve obtained from these mean curves. Fig. b) is an enhanced view of Fig. a). Vertical and horizontal axes are in log scale.

Figure 5:

Effective retention values computed from 200 compost and pozzolan properties for 4 water matric potential values. Crosses represent the mean and ± 1 standard deviations of the 50 computed values per water matric potential

point and the plain line is the mean of the arithmetic mean curves obtained from the compost and pozzolan retention curves used. The vertical axis is in log scale.

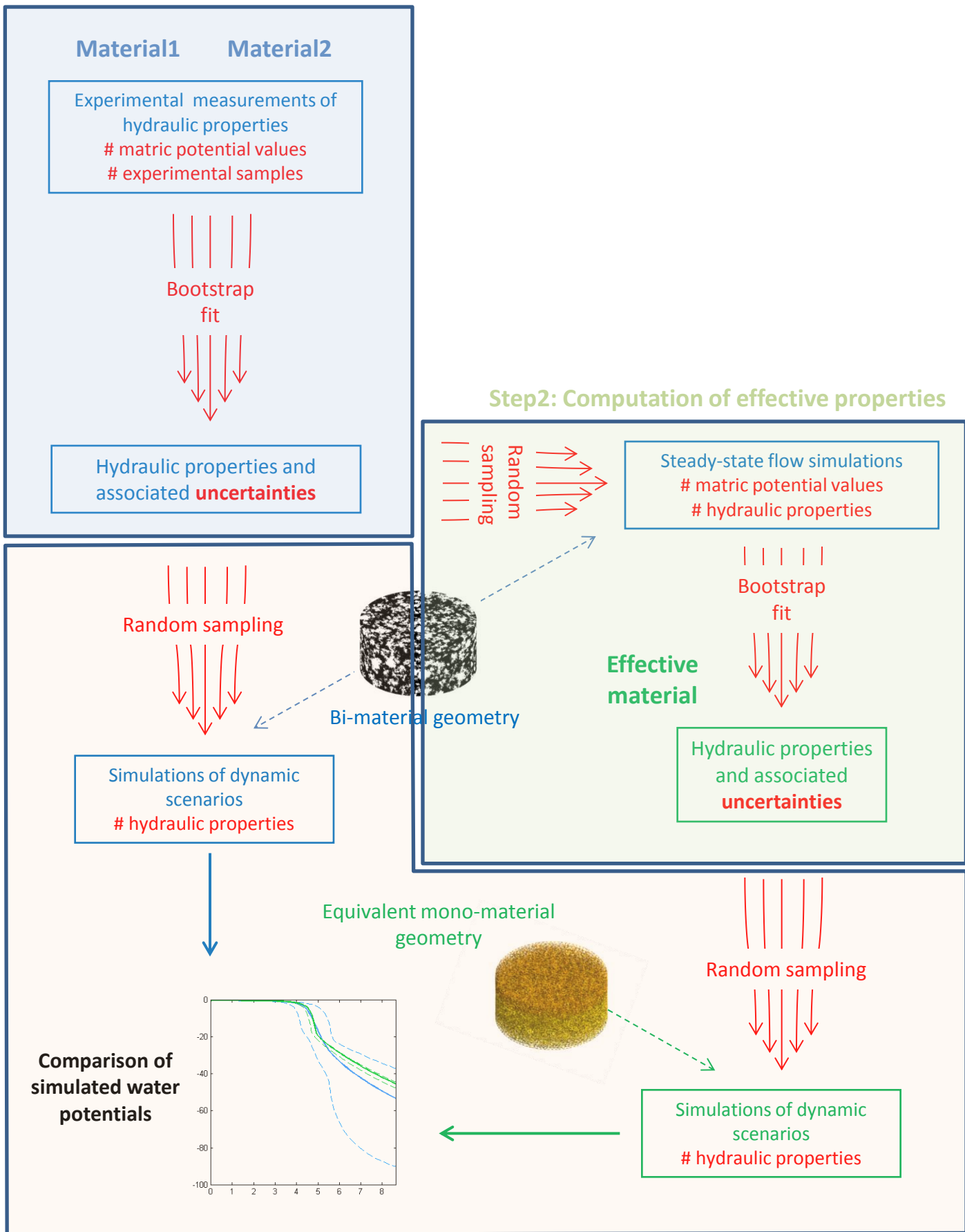
Figure 6:

Snapshots of the evolution of the water potential according to time, at a) $t = 2$ days, b) $t = 6$ days and c) $t = 10$ days. Scales for water matric potential (m) are different for each snapshot.

Figure 7:

Uncertainty distributions of water matric potential values obtained by simulating evaporation using the heterogeneous green roof substrate (black curves) and using the corresponding computed effective homogeneous material (red curves). Dotted or solid curves represent, respectively, 0.5, 99.5 percentile or median values for the water matric potential distributions. The 4 graphs correspond to 4 various depths of the core.

Figure 1
Step1: Estimation of individual material properties



Step3: Evaluation of the homogenization approach

Figure 2

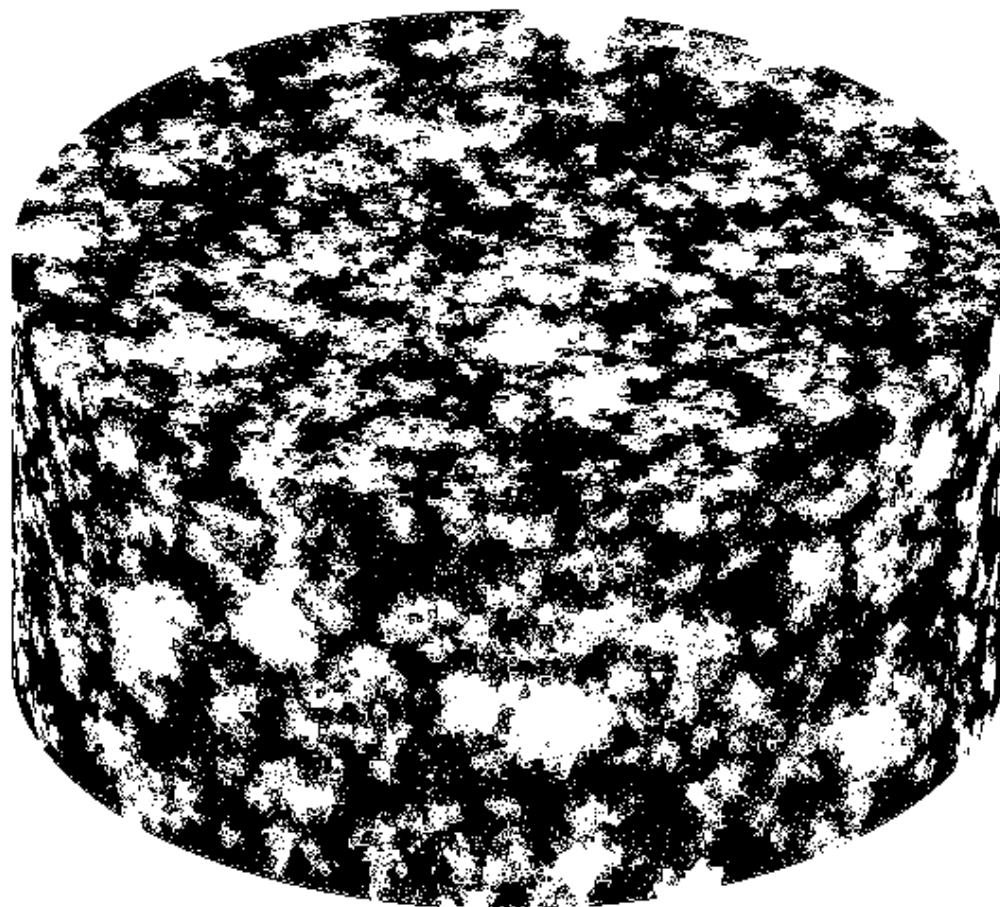
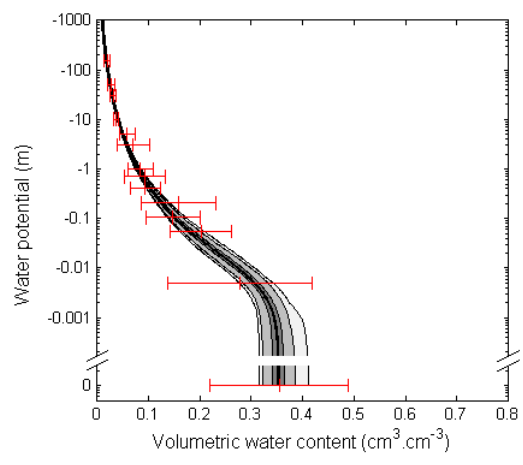
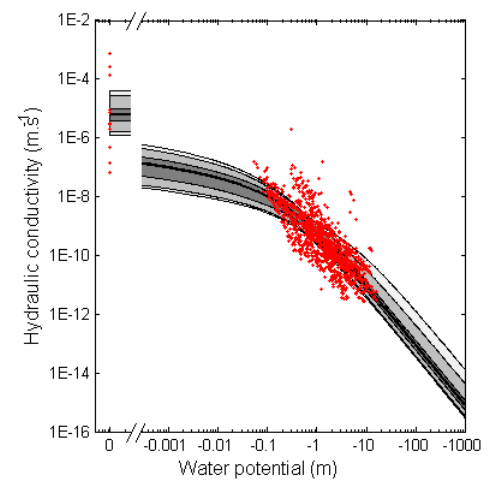


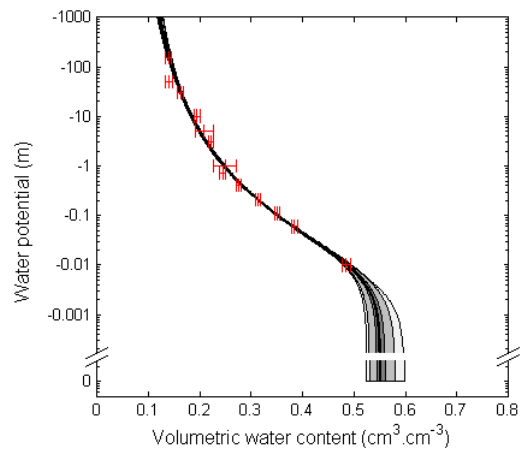
Figure 3



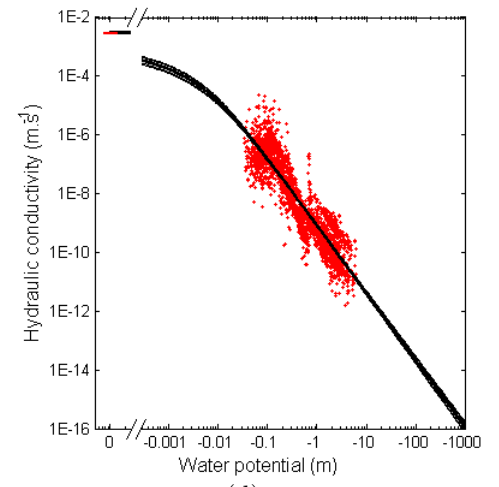
(a)



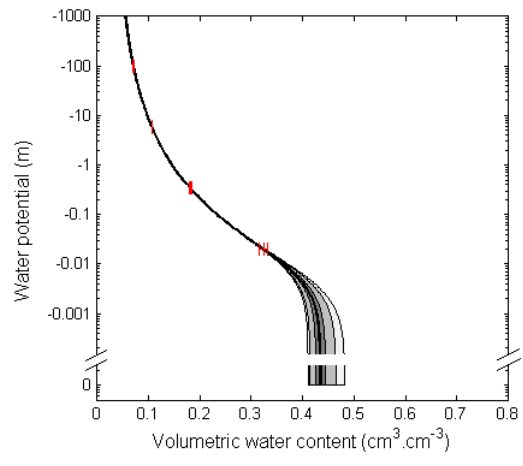
(b)



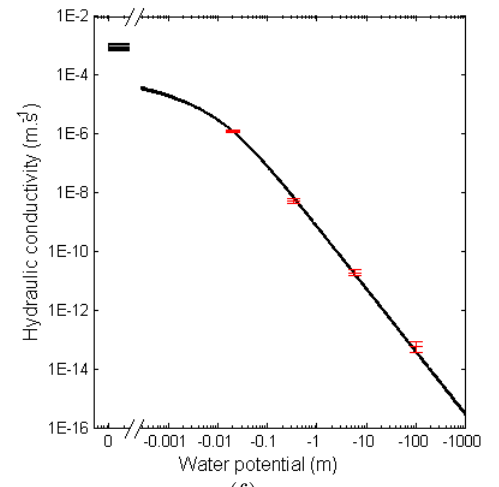
(c)



(d)

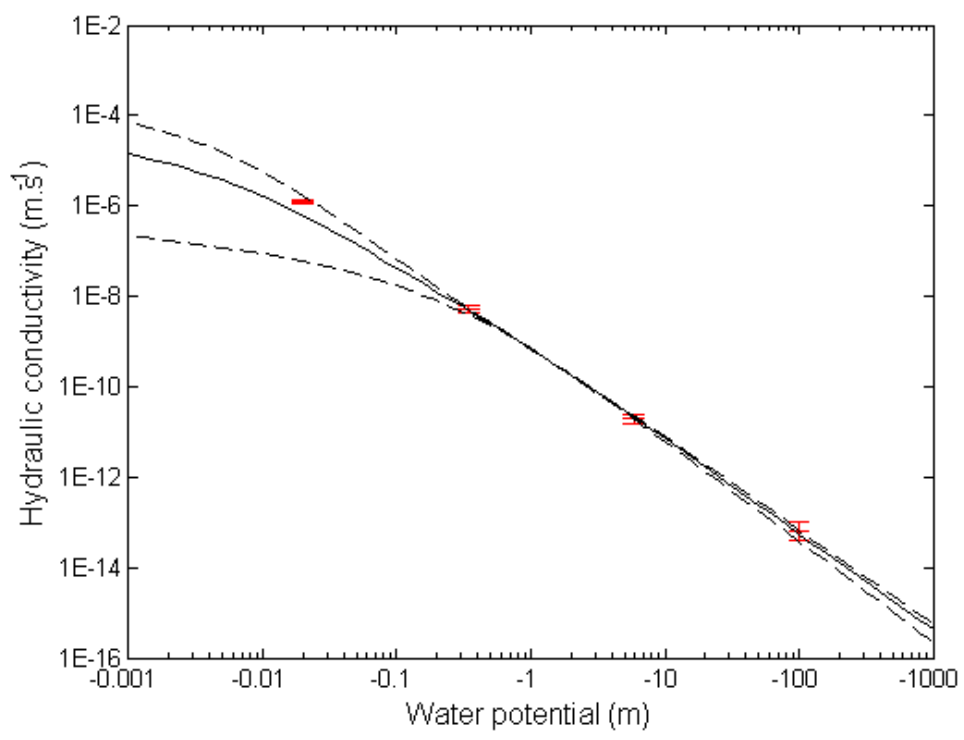


(e)

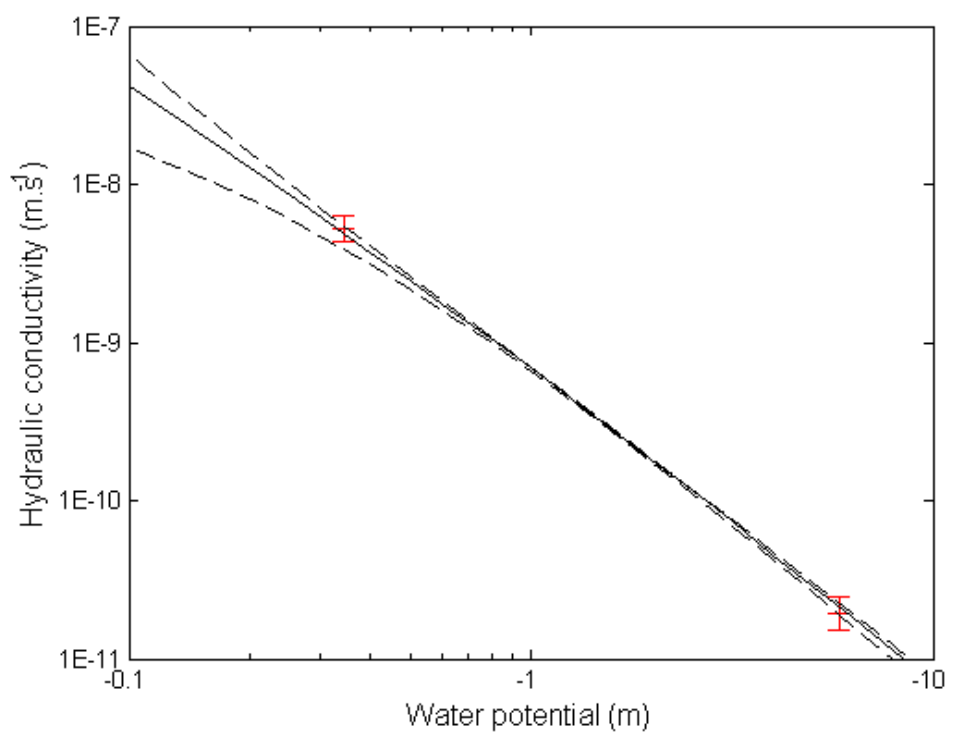


(f)

Figure 4



(a)



(b)

Figure 5

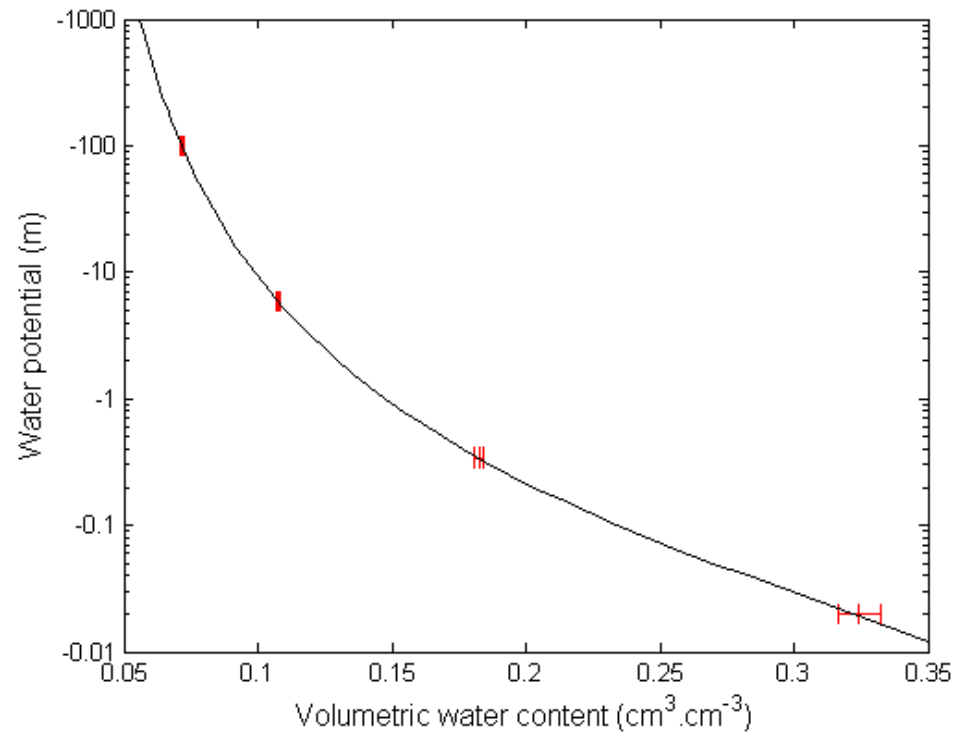
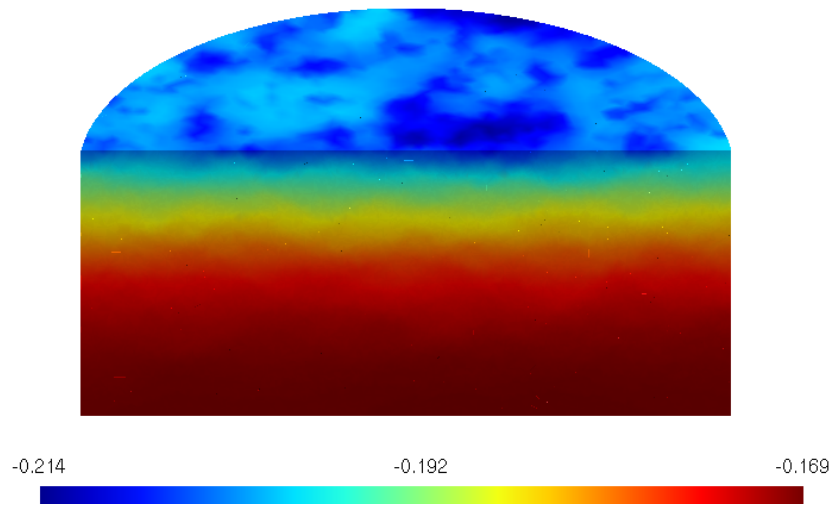
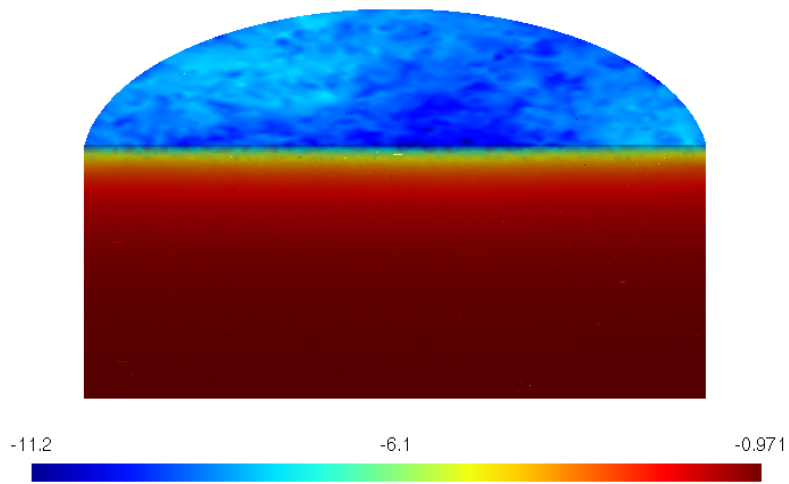


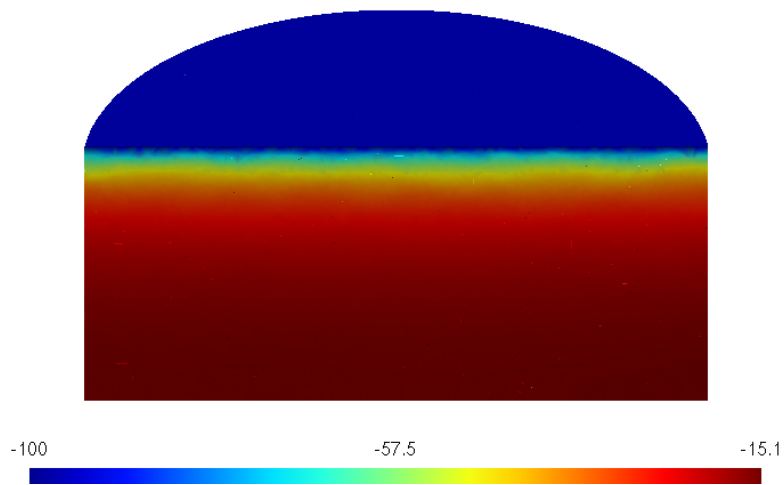
Figure 6



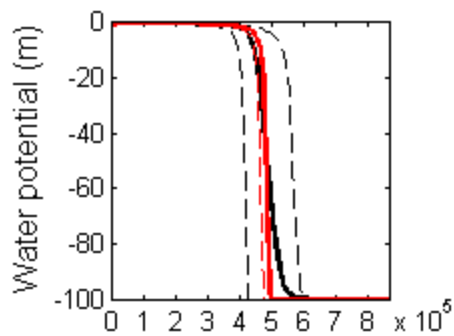
(a)



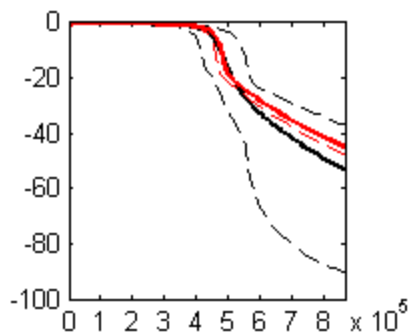
(b)



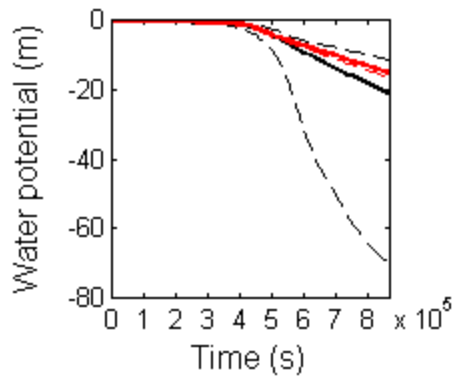
(c)

Figure 7

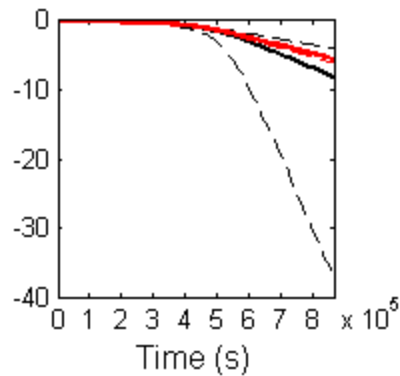
(a)



(b)



(c)



(d)